Author/s:
Mukherjee, S;Perez, KA;Lago, LC;Klatt, S;McLean, CA;Birchall, IE;Barnham, KJ;Masters, CL;Roberts, BR

Title:
Quantification of N-terminal amyloid-β isoforms reveals isomers are the most abundant form of the amyloid-β peptide in sporadic Alzheimer's disease

Date:
2021-01-01

Citation:
Mukherjee, S., Perez, K. A., Lago, L. C., Klatt, S., McLean, C. A., Birchall, I. E., Barnham, K. J., Masters, C. L. & Roberts, B. R. (2021). Quantification of N-terminal amyloid-β isoforms reveals isomers are the most abundant form of the amyloid-β peptide in sporadic Alzheimer's disease. Brain Communications, 3 (2), https://doi.org/10.1093/braincomms/fcab028.

Persistent Link:
https://hdl.handle.net/11343/278084

BRAIN COMMUNICATIONS

Quantification of N-terminal amyloid-β isoforms reveals isomers are the most abundant form of the amyloid-β peptide in sporadic Alzheimer's disease

Soumya Mukherjee,[1] Keyla A. Perez,[1] Larissa C. Lago,[1] Stephan Klatt,[1] Catriona A. McLean,[1,2] Ian E. Birchall,[1] Kevin J. Barnham,[1] Colin L. Masters[1] and Blaine R. Roberts[1,3,4,*]

* Present address: Department of Biochemistry and Department of Neurology, Emory University School of Medicine, 4001 Rollins Research Building, Atlanta, GA 30322, USA.

Plaques that characterize Alzheimer's disease accumulate over 20 years as a result of decreased clearance of amyloid-β peptides. Such long-lived peptides are subjected to multiple post-translational modifications, in particular isomerization. Using liquid chromatography ion mobility separations mass spectrometry, we characterized the most common isomerized amyloid-β peptides present in the temporal cortex of sporadic Alzheimer's disease brains. Quantitative assessment of amyloid-β N-terminus revealed that > 80% of aspartates (Asp-1 and Asp-7) in the N-terminus was isomerized, making isomerization the most dominant post-translational modification of amyloid-β in Alzheimer's disease brain. Total amyloid-β_{1-15} was ~85% isomerized at Asp-1 and/or Asp-7 residues, with only 15% unmodified amyloid-β_{1-15} left in Alzheimer's disease. While amyloid-β_{4-15} the next most abundant N-terminus found in Alzheimer's disease brain, was only ~50% isomerized at Asp-7 in Alzheimer's disease. Further investigations into different biochemically defined amyloid-β-pools indicated a distinct pattern of accumulation of extensively isomerized amyloid-β in the insoluble fibrillar plaque and membrane-associated pools, while the extent of isomerization was lower in peripheral membrane/vesicular and soluble pools. This pattern correlated with the accumulation of aggregation-prone amyloid-β_{42} in Alzheimer's disease brains. Isomerization significantly alters the structure of the amyloid-β peptide, which not only has implications for its degradation, but also for oligomer assembly, and the binding of therapeutic antibodies that directly target the N-terminus, where these modifications are located.

1 Florey Institute of Neuroscience and Mental Health, University of Melbourne, Melbourne, VIC 3010, Australia
2 Department of Anatomical Pathology, Alfred Hospital, Prahran, VIC 3004, Australia
3 Department of Biochemistry, Emory University School of Medicine, Atlanta, GA 30322, USA
4 Department of Neurology, Emory University School of Medicine, Atlanta, GA 30322, USA

Correspondence to: Blaine R. Roberts, PhD
Department of Biochemistry and Department of Neurology, Emory University School of Medicine, Atlanta, GA 30322, USA
E-mail: Blaine.roberts@emory.edu

Keywords: Alzheimer's disease; amyloid-β peptide; long-lived peptide; isomerization; mass spectrometry

Received November 5, 2020. Revised January 9, 2021. Accepted January 15, 2021. Advance Access publication March 9, 2021

Abbreviations: Aβ = amyloid-β; Asp/Asn = aspartate/asparagine; C = control; CCS = drift tube collisional cross-section; ESI = electrospray ionization; ETD = electron transfer dissociation; FA = formic acid; IHC = immunohistochemistry; IMS = ion mobility separations; *m/z* = mass-to-charge ratio; MS = mass spectrometry; PET = positron emission tomography; PRM = parallel reaction monitoring; PTMs = post-translational modifications; SIS = stable isotope standard; SISCAPA = stable isotope standards and capture by anti-peptide antibodies; TBS = tris-buffered saline; UHPLC = ultra-high-performance liquid chromatography

Graphical Abstract

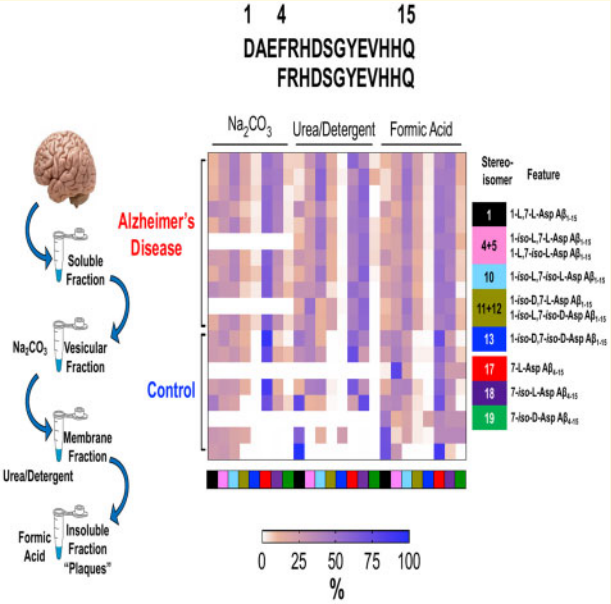

Introduction

Neuropathology and amyloid-β (Aβ) positron emission tomography (PET) studies indicate that the accumulation of Aβ in sporadic Alzheimer's disease brain begins more than 20 years before the onset of clinical symptoms.[1,2] Evidence supports that this accumulation is a result of decreased clearance and not a change in the production of Aβ in sporadic Alzheimer's disease.[3,4] The subtle 2–5% decrease in its clearance results in total accumulation of ~6.5 mg Aβ in the brain over the 20 year time span[2,5] compared to 1.7 mg in age-matched control tissue. However, several questions regarding the Aβ-amyloid hypothesis[6] remain unanswered, including what leads to the decrease in clearance and what triggers the aggregation of Aβ into extracellular plaques[7] along with intracellular tau-reactive neurofibrillary tangles.[8] The impairment in the clearance increases the half-life of the Aβ polypeptide and the process of amyloidosis in Alzheimer's disease entombs the peptide for decades, making it a long-lived peptide. The prolonged time frame of amyloidosis is a common feature across multiple neurodegenerative diseases,[9,10] predisposing the polypeptide chains to undergo multiple spontaneous non-enzymatic post-translational modifications (PTMs), which can render them resistant to normal cellular proteolysis mechanisms.[11,12]

The earliest Edman sequencing and more recent mass spectrometry-based analyses have shown that there is a diverse population of N-terminally truncated species of $A\beta_{42}$ (e.g. $A\beta_{1-42}$, $A\beta_{2-42}$, $A\beta_{4-42}$).[7,13] Moreover, multiple PTMs of Aβ have been described and include nitration,[14] pyroglutamate formation,[15,16] phosphorylation,[17] methionine oxidation,[18] dityrosine cross-linking[19] and structural changes of the polypeptide backbone. Structural changes, in particular, occur on the amino acid level via non-enzymatic, spontaneous processes and facilitated by the amino acids with asymmetric central carbon atom. The most common structural protein modification associated with aging is stereoisomerization of Asp/Asn (aspartate/asparagine) residues and have been particularly useful for protein dating.[20,21] Deamidation of L-Asn residue to L-Asp as well as racemization/isomerization to D-Asp and D/L-*iso*-Asp via succinimide intermediate[22] (Fig. 1A) potentially should provide the information of the age of the Aβ plaques.[23] In Alzheimer's disease brain, the striking feature of the fibrillar Aβ is its sequential N-terminal truncation along with Asp and Ser (serine) epimerization.[13,15,24,25] Qualitative estimates from the plaque-derived Aβ indicate almost 25% of Asp-1 and 75% Asp-7 are isomerized in Alzheimer's disease brains.[9,26–29]

The antibodies currently in clinical trials target multiple forms (soluble oligomeric and insoluble fibrils) of Aβ due

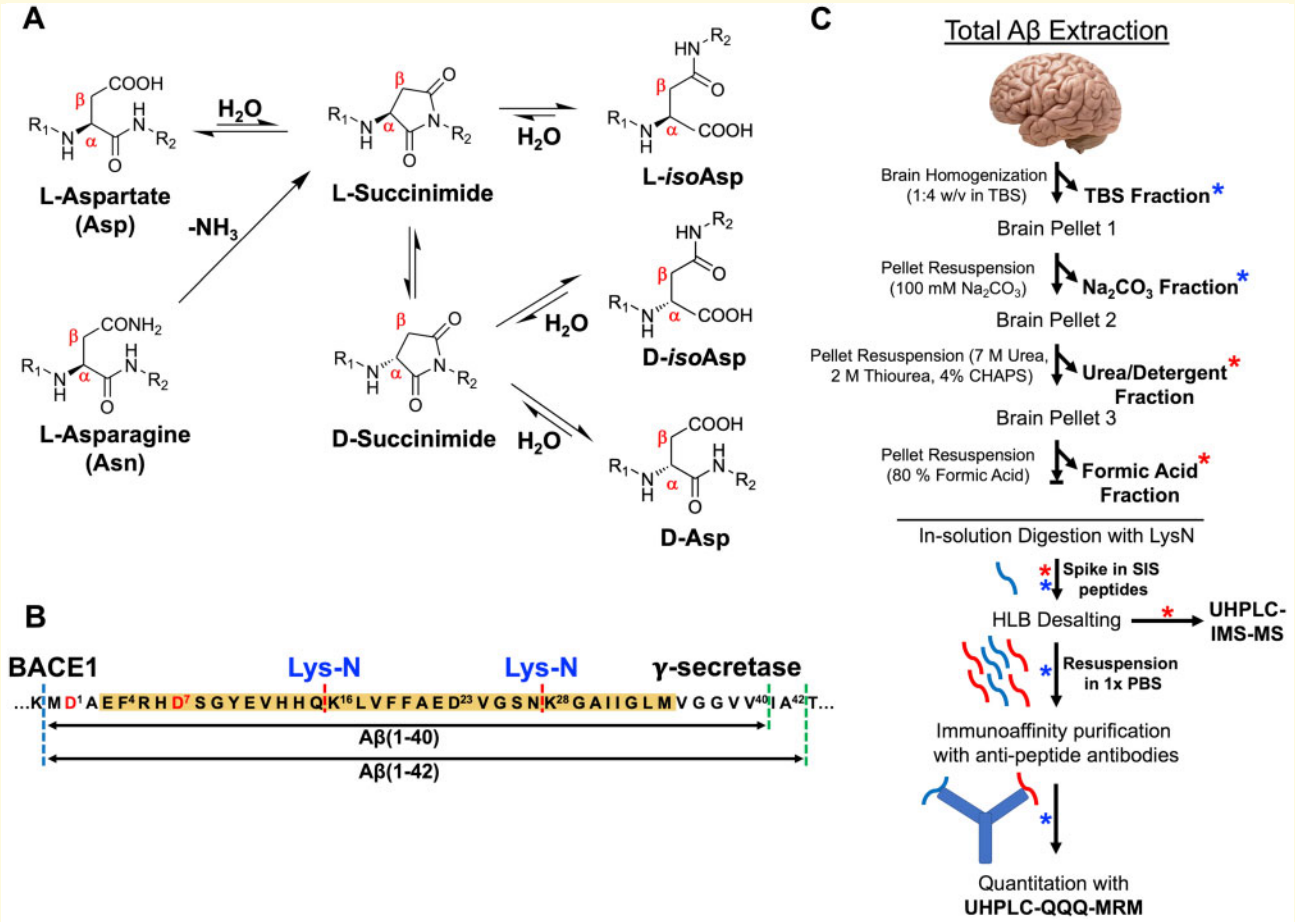

Figure 1 Total amyloid-β extraction from human brain. (**A**) Schematic representation of the spontaneous mechanism of dehydration of L-Asp as well as deamidation of L-Asn forming a succinimide intermediate that subsequently leads to the isomerization/racemization after ring opening to D/L-iso-Asp and D-Asp. (**B**) Amyloidogenic processing of amyloid precursor protein (APP) by β-secretase (dashed blue line) and γ-secretase (dashed green lines) leads to generation of canonical $Aβ_{1–40}$ and $Aβ_{1–42}$ peptides. Proteolytic digestion using LysN enzyme (dashed red line) of the Aβ peptide generates N-terminal, mid-domain and C-terminal fragments that were probed for quantitative evaluation in this study. (**C**) Quantitative proteomics workflow for the estimation of total Aβ in the amyloid rich biochemical pools of the brain after digestion with LysN enzyme and spiking of respective stable isotope standard (SIS) peptides without any enrichment strategy (red asterisk). SISCAPA strategy was used for the sparsely enriched peripheral/vascular (Na_2CO_3) pool and soluble pool (TBS) of Aβ after enzymatic digestion with LysN and spiking with SIS peptides (indicated by blue asterisk).

to their potential roles in the pathogenesis and disease progression.[30,31] Other than the mid-domain and C-terminus Aβ, the other most common target epitope of these antibodies is the PTM-prone N-terminus of Aβ.[32–34] In-depth understanding of the target engagement warrants detailed analysis of the PTMs (especially isomerization) associated with these epitopes. However, comprehensive characterization of these isomers/epimers along with their quantitative estimation is yet to be done in Alzheimer's disease brain compared to age-matched control brains.[29] Identification and quantification of the most relevant stereoisomers/structural isomers of Aβ is challenging. These isomers are structurally similar, which increases the difficulty of chromatographic separation and are indistinguishable to single-stage mass spectrometers (MS) due to their identical mass-to-charge (*m/z*) ratios. Analytical chromatographic separation of N-terminal isomers and epimers of Aβ and their simultaneous characterization using MS/MS fragmentation techniques have been investigated.[35–39] Chiral chromatography was shown to separate synthetic Aβ epimers and isomers containing Asp and Ser residues.[40] Ion mobility separation-mass spectrometry (IMS-MS) is a powerful tool for the analysis and characterization of isomerized and epimerized peptides in the gas phase.[41–45] Recently, synthetic tryptic Aβ peptide isomers have been shown to resolve in IMS-MS using structures for lossless ion manipulations (SLIM).[46,47] Coupling of online LC to SLIM-IMS demonstrated the potential of LC-IMS-MS in resolving challenging peptide isomers.[47]

In this article, we have identified, characterized and quantified the most common isomers of Aβ isoforms

extracted from the temporal cortex of Alzheimer's disease brains by using liquid chromatography (LC) coupled to drift tube IMS-QTOF MS. In particular, we determined Alzheimer's disease-specific changes of the Aβ N-terminal pool in comparison to age-matched control brains; we report the total levels of $Aβ_{1–15}$ and its associated modified isomers. We also quantified the total levels of the most abundant isomers of $Aβ_{4–15}$. As an extension of the previously reported biochemical method,[5] we have further quantified the amount of the two classical C-terminal isoforms of Aβ, i.e. $Aβ_{42}$ and $Aβ_{40}$[13] in the most Aβ-enriched brain compartments. More than 92% of Aβ in *post-mortem* brains is partitioned in the insoluble/fibrillar and detergent soluble phase, while only <7% is extractable as vesicular and soluble.[5] For quantitative estimation of Aβ peptides in these moderately/sparsely enriched pools, we developed stable isotope standards and capture by anti-peptide antibodies (SISCAPA)[48,49] of Aβ with polyclonal antibodies. The distribution of the isomer ratios indicated a pattern of compartmentalization of highly isomerized $Aβ_{1–15}$ and $Aβ_{4–15}$ in the insoluble/fibrillar and membrane pool, with a comparatively lower extent of isomerization in the vesicular and soluble pools. This data allowed us to estimate the accurate biochemical identity and distribution of the spontaneously isomerized Aβ in post-mortem brain. This PTM is intricately associated with slow turnover rates and degradation of Aβ which accumulates over decades in sporadic Alzheimer's disease.

Materials and methods

All LC-MS grade solvents, acetonitrile (ACN), formic acid (FA), trifluoroacetic acid (TFA), acetic acid, isopropanol and urea, thiourea, N, N-Bis(2-hydroxyethyl)glycine (Bicine), 3-[(3-Cholamidopropyl)dimethylammonio]-1-propanesulfonate hydrate (CHAPS), iodoacetamide (IAA), tri-ethyl ammonium bicarbonate buffer, NaCl, Na_2CO_3, Tris buffers were purchased from Merck-Sigma or ThermoFischer Scientific. EDTA-free protease inhibitors from Roche. Bond-Breaker™ tris(2-carboxyethyl)phosphine (TCEP) Solution, neutral pH was from ThermoFischer Scientific. MS-grade metalloprotease LysN from *Grifola frondosa*, and dithiothreitol (DTT) were purchased from ThermoFischer Scientific. Biomasher were purchased from Omni International. The MS vials, Advanced Bio Peptide Mapping C_{18} Column (2.1 × 150 mm, 2.7 µm) and ESI low concentration tune mix used for instrument calibration were obtained from Agilent Technologies (Santa Clara, USA). Oasis HLB µElution 96 well-plates were purchased from Waters. Affinity purification was performed using PureProteome NHS FlexiBind Magnetic Beads from Millipore. Stable isotope standards (SIS) of Aβ peptides DAEF(R + 10)HDS GYEVHHQ, F(R + 10)HDSGYEVHHQ, (K + 8)GAIIGL MVGGVV, (K + 8)GAIIGLMVGGVVIA and K(+8)LVF FAEDVGSN were purchased from New England Peptides (MA, USA) and their concentration determined by amino acid analysis. Stock solutions of SIS Aβ peptides were prepared in 2% ACN, 0.05% TFA to a final concentration of 200 fmol/µL and stored at −20°C. All the isomerized Aβ peptide standards were commercially synthesized and purchased from JPT Peptide Technologies (Germany). All the SIS isomeric Aβ peptides were resuspended in 30% ACN, 0.1% FA at 0.2 nmol/µL which were subsequently diluted to ∼2 pmol/µL in 15% ACN, 0.1% FA and stored at −20°C.

Brain tissue

Twenty post-mortem temporal cortex tissue samples were obtained from the Victorian Brain Bank (Australia). In detail, the cohort consisted of age-matched healthy control brains ($n = 9$), where the number of plaques and tangles were histopathologically analyzed and well below the cut-off values for Alzheimer's disease. No other major neuropathological disease was present. Alzheimer's disease brains ($n = 11$) met the standard criteria for Alzheimer's disease neuropathological diagnosis (Demographic summary Supplementary Table 1). The study followed the ethics committees of the University of Melbourne (Ethics 1750801.3).

Immunohistochemistry

Segments of frontal cortex from the same cases were fixed in 10% neutral buffered formalin and processed by standard histological methods for paraffin embedding and sectioning (8 µm). Sections were deparaffinised, endogenous peroxidase blocked with 5% aqueous hydrogen peroxide (5 min), treated (5 min) with 98–100% FA (Scharlau AC10852500), rinsed and immersed in Tris buffer (0.5 M pH 7.6). Sections were incubated in a 1/100 dilution of Dako anti-amyloid antibody (MO872—clone 6 F/3D) for 60 min at room temperature. Positively labelled Aβ was detected with a peroxidase labelled streptavidin/biotin system (Dako K0675) with a diaminobenzidine chromogen. Sections were counterstained with Harris's haematoxylin, dehydrated and cover-slipped for imaging. Low and high magnification images were obtained with a Leica ICC50 HD camera on a Leica DM 750 binocular microscope.

Tissue homogenization protocol and fractionation

Hemisected freshly frozen post_mortem brain tissue was processed as previously described with some modifications.[5] Briefly, the frozen brains at −80°C were warmed to −20°C on ice and the leptomeningeal vessels were removed. The grey matter was dissected into ∼0.25 g aliquots from temporal cortex (Brodmann's area 21). During dissection process, care was taken to keep the tissues frozen. The tissue was weighed out and was first

bio-mashed through the Biomasher (Omni International) by centrifugation at 14 000 *g* for 1 min at room temperature. To the bio_mashed tissue, Tris-buffered saline (TBS, 50 mM Tris–HCl, 150 mM NaCl, pH 8.5) containing EDTA-free protease inhibitors (Roche) was added at a ratio of 1:4 (tissue: buffer, w/v). This solution was transferred to ultracentrifuge tubes (Beckman Coulter) and centrifuged (Optima MAX-XP from Beckman Coulter) at 100 000 *g* for 30 min at 4°C. The supernatant was collected, referred to as TBS fraction henceforth, and stored on ice until freezing.

The resulting pellet was then resuspended in 100 mM Na_2CO_3 pH 11 (1:4, tissue: buffer) and incubated for 20 min on ice before another ultracentrifugation step at 100 000 *g* was carried out for 30 min at 4°C. The supernatant containing peripheral membrane and vesicular material was recovered into an Eppendorf tube, referred to as Na_2CO_3 fraction.

The pellet resulting from Na_2CO_3 fractionation was resuspended with urea_detergent buffer (7 M urea, 2 M thiourea, 4% CHAPS, 30 mM bicine, pH 8.5) and spun at 100 000 *g* for 30 min at 4°C. The supernatant was aspirated out, referred to as urea_detergent fraction. These three biochemical fractions were then snap frozen in liq. N_2 and stored at −80°C until further processing.

The residual pellet was finally incubated in 200 µL 70% glass-distilled FA (GDFA) for 2 h at room temperature in a fume hood. The FA fractions were spun at 13 200 *g* for 15 min at 4°C and supernatant was collected. The FA fractions (fourth biochemical fraction) were aliquoted into 10 µL portions and snap frozen in liquid N_2, freeze dried in a lyophilizer and stored at −80°C. A summary of the biochemical fractionation procedure can be found in Fig. 1C.

In-solution LysN digestion of formic acid, urea–detergent, Na_2CO_3 and TBS fractions

A total of 10 µL of both lyophilized FA and urea_detergent fractions were re_suspended/diluted to 100 µL in 100 mM tri-ethyl ammonium bicarbonate buffer (TEAB), pH 8.5. Next, the samples were reduced by incubating with dithiothreitol (DTT) to a final concentration of 20 mM at 37°C for 30 min, followed by alkylation using 25 mM iodoacetamide (IAA) in the dark for another 30 min. The samples were then diluted to 200 µL with 100 mM TEAB buffer, pH 8.5 and digested overnight by incubation at 37°C after adding LysN metalloprotease at enzyme: protein ratio of 1:100. The same in-solution digestion process was performed with 50 µL for the Na_2CO_3 and 100 µL for the TBS fractions. The Na_2CO_3 fraction was diluted to 100 µL and the TBS fraction to 170 µL with 8 M urea, 100 mM TEAB buffer (pH 8.5), respectively. Sample reduction and alkylation were carried out as described above. Finally, the two fractions were diluted to 250 µL for proteolytic digestion with LysN. All the proteomic sample processing was performed at pH 8.5. The digestion reaction was quenched by adding 10% FA to a final concentration of 0.1%. The FA and urea_detergent samples were then spiked with 10 µL of SIS Aβ peptides mixture (200 fmol/µL of Aβ NEP peptides), while only 5 µL was spiked into the Na_2CO_3 and TBS samples. The acidified samples were finally loaded onto an Oasis HLB µElution 96 well-plate (Waters). The wells were washed with 250 µL of 0.1% FA, followed by 250 µL of 5% methanol, 0.1% FA. The peptides were finally eluted with two sequential washes of 25 µL of 75% ACN, 0.1% FA. The eluent was lyophilized and stored at −20°C until further processing. The FA and urea_detergent samples were re-constituted in 25 µL of 2% ACN, 0.05% TFA, vortexed for 30 min on ice and sonicated for 2 min. The re-constituted samples were centrifuged at 10 000 *g* for 5 min and the supernatant was aliquoted in MS vials (Agilent Technologies) for analysis.

Generation of anti-peptide antibodies

An integrated commercial procedure (New England Peptides, MA, USA) was used to generate affinity purified rabbit polyclonal antibodies against Lys-N cleaved $Aβ_{1–40}$ and $Aβ_{1–42}$ peptide sequences (Fig. 1B), i.e. $Aβ_{1–15}$, $Aβ_{4–15}$, $Aβ_{16–27}$, $Aβ_{28–40}$ and $Aβ_{28–42}$. The lyophilized antibodies were re-constituted in 0.05% azide solution at ∼1 mg/mL with shaking for 1 h on ice and aliquoted into vials to avoid repeated freeze-thaw cycles and stored at −80°C.

Aβ SISCAPA (stable isotope standards and capture by anti-peptide antibodies)

Enrichment experiments were performed in a round-bottom 96-well polypropylene plates using the magnetic bead protocol. The NEP Aβ anti-peptide antibodies were coupled to PureProteome NHS FlexiBind Magnetic Beads (Millipore) according to the manufacture's protocol. At first, the capture efficiencies of the anti-peptide antibodies were determined in a complex background. Lyophilized LysN-digested pooled brain homogenate (10 µg total digested protein) was resuspended in 200 µL with PBS, 0.03% CHAPS pH 7.5 buffer along with the 500 fmol of respective SIS Aβ peptides and 1 µg of specific antibody (Supplementary Fig. 1). These antibodies specifically captured LysN-cleaved versions of Aβ peptides with no cross-reactivity for tryptic-cleaved versions.

For the multiplexed experiment, 1 µg of each antibody was added to the sample mixture and 1 M Tris–HCl pH 7.5 to a final concentration of 0.2 mM. To this mixture, 500 fmol SIS Aβ peptides were added. The mixture was incubated overnight at 4°C with shaking at 800 rpm.

After overnight incubation the magnetic beads were magnetized, and the supernatant was discarded. Next, the magnetic beads were manually washed three times with 0.1 M ammonium acetate, 0.5 M NaCl, 0.03% CHAPS (pH 7.5) followed by another three washes with 0.1 M ammonium acetate, 15% ACN, pH 7.5. Finally, the captured peptides were eluted from the magnetic beads with 25 µL of 5% acetic acid, 15% ACN with shaking at 600 rpm and 2 min incubation.

This SISCAPA process was used only on the LysN-digested lyophilized Na_2CO_3/TBS brain fractions for Aβ enrichment.

LC-drift tube ion mobility mass spectrometry

An Agilent 1290 Infinity series UHPLC system coupled to Agilent 6560 Drift Tube Ion Mobility QToF high-resolution MS (Agilent Technologies, Santa Clara, USA) was used for UHPLC-ESI-IM-MS separations. 0.1% FA in water (mobile phase A) and 0.1% FA in 100% ACN (mobile phase B) were used as a solvent system. Samples were loaded onto an Agilent Advanced Bio Peptide Mapping C_{18} Column (2.1 × 150 mm, 2.7 µm) through ultra-low dispersion kit (5067–5963 Agilent Technologies), maintained at 60°C in thermostatted column compartment (TCC) and eluted at 0.4 mL/min flow rate with the following linear gradient: *t* (min), % B: 0, 2.5; 5,6; 64, 22; 85, 29; 90, 34; 95, 81; 97, 81; 97, 2.5; stop time, 99 min. The ESI source parameters operating in positive ion mode were as follows; gas temp., 300°C; drying gas, 6 L/min; nebulizer, 35 psi; sheath gas temp., 275°C, sheath gas flow, 12 L/min; *V*cap, 4500 V. The peptides were analyzed in the positive 4-bit multiplexing IM-QTOF mode in the *m/z* range of 290–1700 with a maximum drift time of 50 ms using nitrogen as drift gas, trap fill time of 3.2 ms; trap release time of 0.3 ms, and acquisition rate of 1 IM frame/s. The drift tube was operated with an absolute entrance voltage of 1700 V and an exit voltage of 250 V (drift field 18.529 V/cm) and the trapping funnel RF was set at 150 V. An Agilent ESI-Low Calibration mixture was injected both before the analysis to tune the instrument in the *m/z* range of 100–1700 and at the start of the worklist to perform single-field Collisional Cross Section ($^{DT}CCSN_2$) recalibration. The drift gas upgrade kit maintained both the drift tube and trap funnel pressure at constant 3.94 ± 0.01 and 3.80 ± 0.02 Torr, respectively, while the drift tube ambient temperature was stable at 23.5 ± 0.3°C across all the acquisition runs.

LC-QQQ-MRM mass spectrometry

An Agilent 1200 Infinity series UHPLC system connected to 6495 QQQ (Agilent Technologies, USA) was used for the LC-ESI-QQQ-MRM assay. Mobile phase A consisted of 0.1% FA in water and mobile phase B of 0.1% FA in 100% ACN. Samples were loaded onto an Advanced Bio Peptide Mapping C_{18} Column (2.1 × 150 mm, 2.7 µm) maintained at 55°C in TCC and eluted at 0.4 mL/min flow rate with the following gradient, 2.5% B, 0 min; 6% B, 5 min; 9% B, 20 min; 22% B, 25 min; 29% B, 35 min; 34% B, 37 min; 81% B, 38 min; 81% B, 40 min; 2.5% B, 41 min with a post-run equilibration for 2 min. The list of transitions along with their retention times (RT) are presented in Supplementary Table 2. The source ESI parameters as well the collision energies were optimized for these peptides in the positive ion mode. The typical parameters were: gas temperature 200°C, gas flow 15 L/min, nebulizer 40 psi, sheath gas temperature 250°C and sheath gas flow 11 L/min. The capillary voltage was 4500 V and the nozzle voltage was set at 1000 V. The optimized iFunnel parameters were 150 and 60 V for high- and low-pressure RF, respectively. A total of 20 µL of LysN digested Na_2CO_3 SISCAPA samples were injected on to the columns.

Data processing and statistical analyses

The IMS-MS data files collected using 4-bit multiplexing mode were first de-multiplexed using vendor-supplied software without any smoothing applied.[50] Data post-processing, including $^{DT}CCSN_2$ calibration and feature finding was carried out using IM-MS browser and Mass Profiler from MassHunter Suite (B.08.00, Agilent Technologies, Santa Clara, USA). Following post-processing, the raw data were imported into Skyline (v4.2) with formula annotations of the targeted peptides added to the method. Data for each peptide was extracted in the software in a MS1 filtering mode[51] using the accurate mass of the top three isotopic peaks, drift time and RT for the precursor list workflow. The peak abundance for the $Aβ_{1–15}$, $Aβ_{4–15}$, $Aβ_{16–27}$, $Aβ_{28–40}$ and $Aβ_{28–42}$ peptides in this study were performed on the first three peaks of the isotope cluster. The peak areas of the endogenous peptides and their heavy analogues (R = $^{13}C_6$, $^{15}N_4$, K = $^{13}C_6$, $^{15}N_2$) were extracted to derive the light-to-heavy ratios. The absolute quantification was determined by comparing the peak areas of the SIS peptides.

For the drift tube IMS, the resolving power R and resolution r are defined as $R = t_d/w$ and $r = 1.18 * (t_{d1} - t_{d2})/(w_1 + w_2)$, where t_d is the drift time of the ion and w is the full peak width at half-maximum (FWHM). To determine statistically significant differences between potential biomarkers (healthy versus Alzheimer's disease brain tissue), the unpaired independent sample *t*-test was used, while Pearson's correlation was used to assess correlation between different cell fractions. For the total amount of isomers and their normalized ratio, adjusted *P* values were calculated with one-way analysis of variance (ANOVA), corrected for multiple comparison false discovery rate ($P < 0.05$) with Benjamini–Hochberg correction. The means of most common isomers of $Aβ_{1–15}$

and $A\beta_{4–15}$ were summarized as pie charts for Alzheimer's disease and control brains, respectively, obtained from different biochemical fractions.

The degree of amyloid pathology was assessed in the *post-mortem* temporal cortex tissue using anti-Aβ immunohistochemistry (IHC) and semi-quantitatively scored by an independent assessor (CAM) after anti-Aβ (aa 8–17; 6 F/3D) staining. The scoring system comprised of; the following four categories: −, absent or not discernible, +, slight; ++, moderate; +++, severe. The semi-quantitative IHC scores were compared with the quantitative results obtained using IMS-MS in this study.

Data availability

Patient and post-mortem brain tissue demographics, experimental details of nano-LC-ESI-MS/MS for ETD-PRM, MRM transition list for Aβ SISCAPA on QQQ, age-of-death correlation with absolute quantity of Aβ peptides and the respective isomers are provided in the supporting information. Additional data related to this article may be requested from the authors.

Results

Characterization of epimerization of Asp residues in brain-derived Aβ

Qualitative bottom-up proteomic identification of Aβ peptides in Alzheimer's disease brain tissue demonstrated a range of N-terminal truncations including $A\beta_{1–15}$, $A\beta_{2–15}$, $A\beta_{3Glu-15}$, $A\beta_{4–15}$ and the two canonical C-terminal peptides, $A\beta_{28–40}$ and $A\beta_{28–42}$ (Supplementary Table 3).[13] Previous reports characterizing stereoisomers of synthetic Aβ have particularly demonstrated that isomerization at position Asp-1 and Asp-7 is frequent.[23,38,52] However, neither the extent of isomerization of Asp-1 and Asp-7 residues in $A\beta_{1–15}$, $A\beta_{2–15}$, $A\beta_{3Glu-15}$ and $A\beta_{4–15}$ have been directly measured in human brain nor has a systematic study been conducted using ion mobility to determine the effect of isomerization on the structure of these peptides in the gas phase. We postulated that the orthogonality of the online LC and drift tube ion mobility separations (DT-IMS) would provide the required analytical resolution, even if at modest $R \sim 50$, to resolve the N-terminal Aβ isomers/racemers derived from Alzheimer's disease brains and improve the detection/quantification limits of these complex biological samples. We applied DT-IMS in combination with chromatography and synthetic heavy labelled Aβ standards to characterize the identity of isomerized $A\beta_{1–15}$, $A\beta_{2–15}$, $A\beta_{3Glu-15}$ and $A\beta_{4–15}$ from Alzheimer's disease brain.

As $A\beta_{1–15}$ has two Asp residues (Asp-1 and Asp-7) that can undergo individual isomerization/epimerization events, each peptide having combination of their L/D and/or *iso*-L/*iso*-D forms resulting in total 16 $A\beta_{1–15}$ isomers. Hence, we systematically characterized the liquid chromatography retention time (LC-RT) and $^{DT}CCSN_2$ properties of possible synthetic SIS $A\beta_{1–15}$ peptides (Supplementary Fig. 2). Next, probable combinations of different isomers were spiked into the proteolytically digested FA fraction extracted from an Alzheimer's disease brain (Supplementary Fig. 3). The alignment of the drift times of the endogenous $[M+4H]^{4+}$ *m/z* 457.4515 ion and the predicted SIS isomer $[M+4H]^{4+}$ *m/z* 459.9535 ion in IMS-MS (Supplementary Fig. 3) along with the chromatographic elution (Supplementary Fig. 4) confirmed the identities of the endogenous $A\beta_{1–15}$ isomer. Based on chromatographic RT and averaged $^{DT}CCSN_2$ (Fig. 2A), we were able to characterize the most abundant seven isomers of $A\beta_{1–15}$ found in the FA fraction of Alzheimer's disease brain (with increasing RT) as 1-L, 7-L-Asp (1); 1-*iso*-L, 7-L-Asp (4); 1-L, 7-*iso*-L-Asp (5); 1-*iso*-L, 7-*iso*-L-Asp (10); 1-*iso*-D, 7-*iso*-L-Asp (11); 1-*iso*-L, 7-*iso*-D-Asp (12) and 1-*iso*-D, 7-*iso*-D-Asp (13). Minor singly enantiomerized $A\beta_{1–15}$ epimers present in the Alzheimer's disease FA fraction (with increasing RT) were 1-D, 7-L-Asp (2) and 1-*iso*-L, 7-D-Asp (3); 1-*iso*-D, 7-D-Asp (6), 1-D, 7-*iso*-L-Asp (7) and 1-*iso*-D, 7-L-Asp (8) (Fig. 2A). The $^{DT}CCSN_2$ of $[M+4H]^{4+}$ ions for $A\beta_{1–15}$ epimers indicated a trend in ion mobility from D-Asp < L-Asp < *iso*-D-Asp < *iso*-L-Asp. The $^{DT}CCS_{N2}$ also indicated that the N-terminal Asp-1 epimerization does not significantly influence the gas phase structure (Fig. 2D) compared to the natural 1-L, 7-L-Asp $A\beta_{1–15}$ (1) peptide. However, internal Asp-7 isomerization not only influences the RT of the isomerized species compared to the natural 1-L, 7-L-Asp (1) $A\beta_{1–15}$ peptide, but importantly leads to a significant increase in $^{DT}CCS_{N2}$ ($\Delta^{DT}CCS_{N2} \sim 10$, Fig. 2A). This indicates a change in the gas phase conformation for the $[M+4H]^{4+}$ ion of the Asp-7 isomerized $A\beta_{1–15}$ peptides in comparison with its native form.

On closer inspection, unmodified 1-L, 7-L-Asp (1) and 1-D, 7-D-Asp (15) epimers had similar RT (Fig. 2A, highlighted) but were slightly distinguishable in DT-IMS with $^{DT}CCS_{N2}$ 606 Å^2 (Fig. 2a, black) and 601 Å^2 (Fig. 2A, violet), respectively. Although a DT resolution of $r \sim 0.4$ ($R \sim 60$) between 1-L, 7-L-Asp (1) ($t_d = 20.2$ ms) and 1-D, 7-D-Asp (15) ($t_d = 19.7$ ms) epimers (Fig. 2A, inset) is not sufficient for baseline resolution ($r \sim 1.5–2$ is optimal for baseline separation), the presence of both of these species would have led to a DT peak broadening for the endogenous $[M+4H]^{4+}$ *m/z* 457.4515 ion. However, DT-IMS results indicated doubly racemized endogenous $A\beta_{1–15}$ (Fig. 2A, inset) is not present above the limit of detection.

Similarly, we characterized the isomers of other common N-truncated isoforms of Aβ derived from Alzheimer's disease brains (Fig. 2B–D, Supplementary Fig. 5). In particular, 2D-LC-IMS-MS correlation of the endogenous $A\beta_{4–15}$ $[M+4H]^{4+}$ peptide with its synthetic isomerized standards demonstrated that along with unmodified 7-L-Asp (17), 7-*iso*-L-Asp (18) and 7-*iso*-D-Asp (19) are the primary isomers of $A\beta_{4–15}$ present in

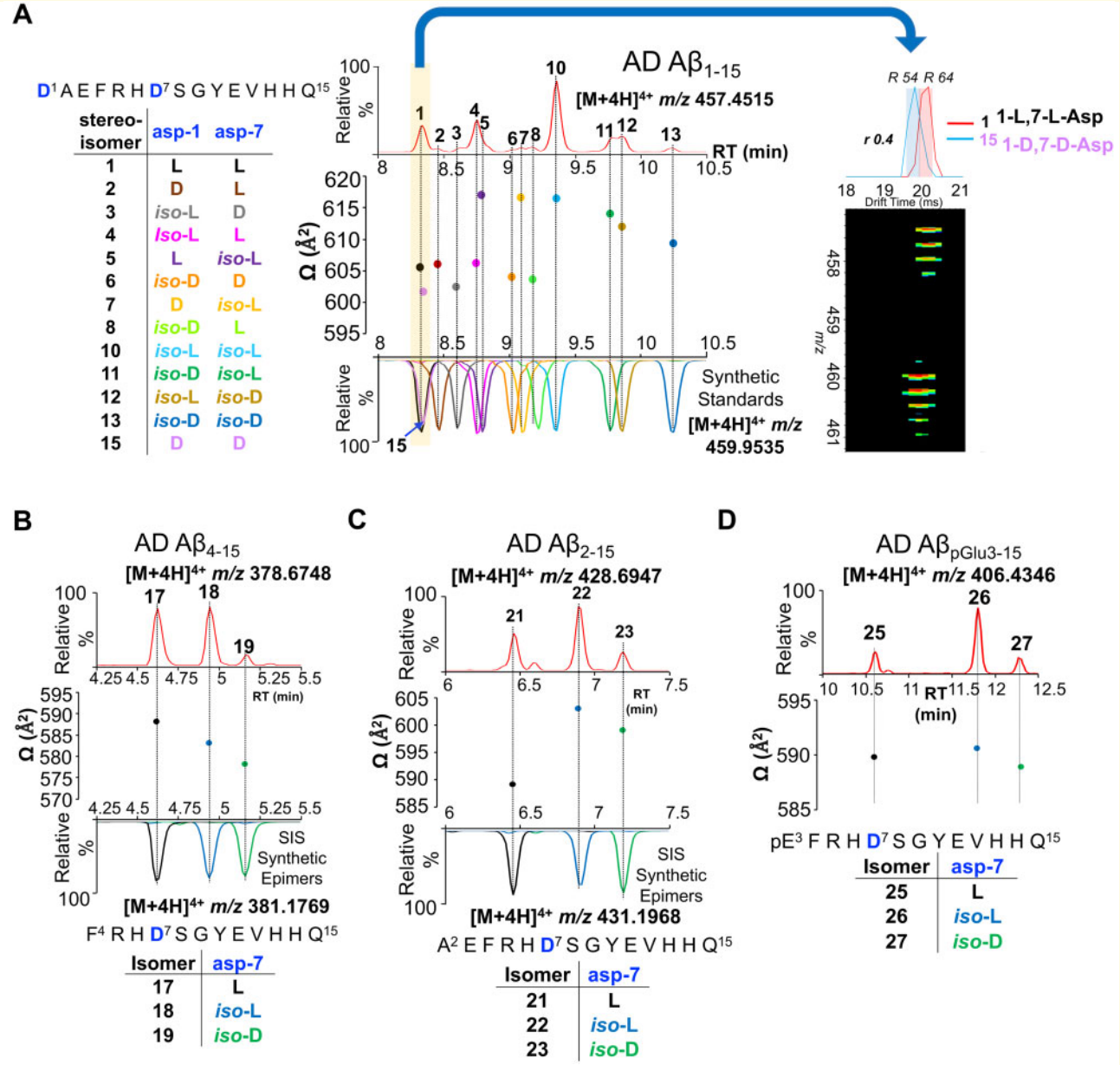

Figure 2 Ion-mobility of amyloid-β isomers. Two-dimensional representation of RT_ion mobility high-resolution mass spectrometry (2D-LC-IMS-MS) results of extracted ion chromatograms (EIC) of N-terminal Aβ peptides present in Alzheimer's disease brain. (**A**) 2D-LC-IMS-MS of $A\beta_{1-15}$ $[M+4H]^{4+}$ *m/z* 457.4515 from formic acid fraction of human Alzheimer's disease case illustrating the diversity of the isomerized Asp-1 and Asp-7 residues. The most abundant endogenous isomer of $A\beta_{1-15}$ (*top red panel*) were characterized by comparing their chromatographic separation (co-elution) and their $^{DT}CCSN_2$ (Å^2) with the synthetic standards (*bottom multiple colour panel*). The alignment of both the LC as well as the $^{DT}CCS_{N2}$ (Å^2) reveal the most abundant endogenous isomers of $A\beta_{1-15}$ in the FA fraction are 1,7-L-Asp (1), 1-*iso*-L, 7-L-Asp (4), 1-L, 7-*iso*-L-Asp (5), 1-*iso*-L, 7-*iso*-L-Asp (10), 1-*iso*-D, 7-*iso*-L-Asp (11), 1-*iso*-L, 7-*iso*-D-Asp (12) and 1-*iso*-D, 7-*iso*-D-Asp (13). The epimerized peptides 1-D, 7-L-Asp (2), 1-*iso*-L, 7-D-Asp (3), 1-*iso*-D, 7-D-Asp (6), 1-D, 7-*iso*-D-Asp (7) and 1-*iso*-D, 7-L-Asp (8) are minor constituents. The highlighted (yellow) LC-MS region depicts co-elution of native 1-L, 7-L-Asp (1) and 1-D, 7-D-Asp (15) at 8.3 min, although minute $\Delta^{DT}CCS_{N2} \sim 5$ indicates that endogenous species corresponds to 1-L, 7-L-Asp (1) native $A\beta_{1-15}$. (**B**) 2D-LC-IMS-MS representation of endogenous $A\beta_{4-15}$ $[M+4H]^{4+}$ *m/z* 378.6748 (top *red panel*) compared to isomerized synthetic standards (*bottom panel*), (**C**) $A\beta_{2-15}$ $[M+4H]^{4+}$ *m/z* 428.6947 (*top red panel*) compared to isomerized synthetic peptide standards (*bottom panel*) and (**D**) endogenous $A\beta_{pGlu3-15}$ $[M+4H]^{4+}$ *m/z* 406.4328 (*top LC panel*, red). $^{DT}CCS_{N2}$ (Ω in Å^2) are shown for the corresponding isomerized peptides for clarity.

Alzheimer's disease brain (Fig. 2B, Supplementary Fig. 5 A). For $A\beta_{2-15}$ $[M+4H]^{4+}$, the most common isomers were 7-*iso*-L-Asp (22) and 7-*iso*-D-Asp (23) along with unmodified 7-L-Asp (21) (Fig. 2C, Supplementary Fig. 5B). Based on the RT and trend in $^{DT}CCSN_2$ of the above-characterized epimers/isomers of the three

N-terminal Aβ peptides ($Aβ_{1–15}$, $Aβ_{4–15}$ and $Aβ_{2–15}$), we predicted the major isomers of $Aβ_{pGlu3–15}$ as 7-L-Asp (25), 7-*iso*-L-Asp (26) and 7-*iso*-D-Asp (27) with increasing RT (Fig. 2D, Supplementary Fig. 5 C). This was further confirmed by the diagnostic *iso*-Asp-7 ions generated via electron transfer dissociation-parallel reaction monitoring (ETD-PRM) (Supplementary Fig. 6 and Dataset 1).

Similar to $Aβ_{1–15}$ isomers, internal Asp-7 isomerization of $Aβ_{2–15}$ led to a larger $^{DT}CCS_{N2}$ for the $[M+4H]^{4+}$ *m/z* 428.6934 compared to unmodified 7-L-Asp (21) peptide. In contrast, the $[M+4H]^{4+}$ *m/z* 378.6791 *iso*-Asp-7 $Aβ_{4–15}$ peptide isomer was more compact (smaller $^{DT}CCS_{N2}$) compared to its unmodified version (Fig. 2B). No change in $^{DT}CCS_{N2}$ (Fig. 2D, Supplementary Fig. 5 C) for the $[M+4H]^{4+}$ *m/z* 406.4329 *iso*-Asp-7 $Aβ_{pGlu3–15}$ isomer was observed compared to its unmodified peptide. The structural reorganization inside the peptide backbone due to isomerization influences the shape and size of these peptides in the gas phase. N-truncation along with the loss of basic amino acid residues might further influence the charge distribution of these isomerized peptide ions that can lead to $^{DT}CCS_{N2}$ alteration compared to unmodified Asp-L peptides.

We also investigated if the mid-region peptide $Aβ_{16–27}$ derived from Alzheimer's disease brain exhibited any conformational changes due to Asp-23 isomerization, as previously proposed.[9] The presence of a single endogenous $Aβ_{16–27}$ species from Alzheimer's disease brain indicated no isomerization, verified by ETD-PRM (Supplementary Fig. 7 A) and 2D-LC-IMS-MS ($^{DT}CCS_{N2}$ ~ 387 Å^2) (Supplementary Fig. 7B). Similarly, no isomerization for the endogenous C-terminal peptides $Aβ_{28–40}$ ($^{DT}CCS_{N2}$ ~ 372 Å^2) and $Aβ_{28–42}$ ($^{DT}CCS_{N2}$ ~ 406 Å^2) were detected in Alzheimer's disease brain (Supplementary Fig. 7B).

Absolute quantitation of N-terminal Aβ peptides and estimation of Asp-1 and Asp-7 isomerization

Absolute quantitation of the $Aβ_{1–15}$ and $Aβ_{4–15}$ peptides in each of the four biochemical fractions of Alzheimer's

Table 1 Demographics and quantitation of Aβ from frontal cortex

	Alzheimer's disease (*N* = 11)	Control (*N* = 9)	*P*
Age (years)	84.19 (11.35)	69.90 (10)	0.01
PMI (h)	29.5 (20.2)	47.5 (22.8)	0.07
Formic acid (fmol/mg brain)			
$Aβ_{1–15}$	207.8 (154.1)	11.43 (11.35)	0.0024
$Aβ_{4–15}$	89.03 (56.68)	6.47 (7.67)	0.0004
$Aβ_{16–27}$	4345 (1833)	368.0 (421.2)	<0.0001
$Aβ_{28–40}$	326.1 (540.3)	5.63 (10.96)	0.1144
$Aβ_{28–42}$	2278 (1090)	233.7 (303.0)	0.0003
$Aβ_{28–42}/Aβ_{28–40}$	44.75 (43.51)	97.47 (135.3)	0.2448
Urea-detergent (fmol/mg brain)			
$Aβ_{1–15}$	76.63 (41.47)	4.10 (3.53)	0.0008
$Aβ_{4–15}$	10.84 (6.32)	0.44 (0.66)	0.0001
$Aβ_{16–27}$	817.9 (732.1)	198.5 (204.4)	0.036
$Aβ_{28–40}$	24.44 (57.69)	1.69 (4.27)	0.2848
$Aβ_{28–42}$	906.0 (692.8)	242.4 (255.8)	0.0207
$Aβ28_{–42}/Aβ_{28–40}$	1241 (2364)	2368 (3396)	0.3936
Na_2CO_3 (fmol/mg brain)			
$Aβ_{1–15}$	16.16 (9.78)	4.0 1(1.72)	0.0021
$Aβ_{4–15}$	10.91 (6.7)	0.86 (1.32)	0.0004
$Aβ_{16–27}$	118.0 (76.73)	25.0 (20.30)	0.0047
$Aβ_{28–40}$	5.92 (7.89)	2.48 (0.51)	0.2102
$Aβ_{28–42}$	33.61 (19.87)	9.39 (7.28)	0.0001
$Aβ_{28–42}/Aβ_{28–40}$	8.02 (4.08)	3.96 (3.16)	0.0311
TBS (fmol/mg brain)	**Alzheimer's disease (*N* = 9)**	Control (*N* = 9)	
$Aβ_{1–15}$	16.4 (0.9)	4.92 (1.0)	0.0365
$Aβ_{4–15}$	2.01 (0.79)	0.07 (0.03)	0.0263
$Aβ_{16–27}$	22.28 (4.93)	7.34 (2.3)	0.0093
$Aβ_{28–40}$	1.23 (0.54)	0.56 (0.47)	0.2572
$Aβ_{28–42}$	0.18 (0.2)	0.05 (0.01)	0.3960
$Aβ_{28–42}/Aβ_{28–40}$	0.29 (0.46)	0.18 (0.16)	0.7225
Total (fmol/mg brain)	**Alzheimer's disease (*N* = 11)**	**Control (*N* = 9)**	
$Aβ_{1–15}$	297.7 (193.5)	16.9 (15.73)	0.0009
$Aβ_{4–15}$	108.8 (66.42)	7.78 (9.28)	0.0008
$Aβ_{16–27}$	5260 (2190)	525.8 (614)	<0.0001
$Aβ_{28–40}$	355.4 (599.6)	8.99 (14.95)	0.0844
$Aβ_{28–42}$	3211 (1156)	406.6 (502.9)	<0.0001

All values are mean values (±SD); significance was determined by unpaired *t*-test with equal variance.

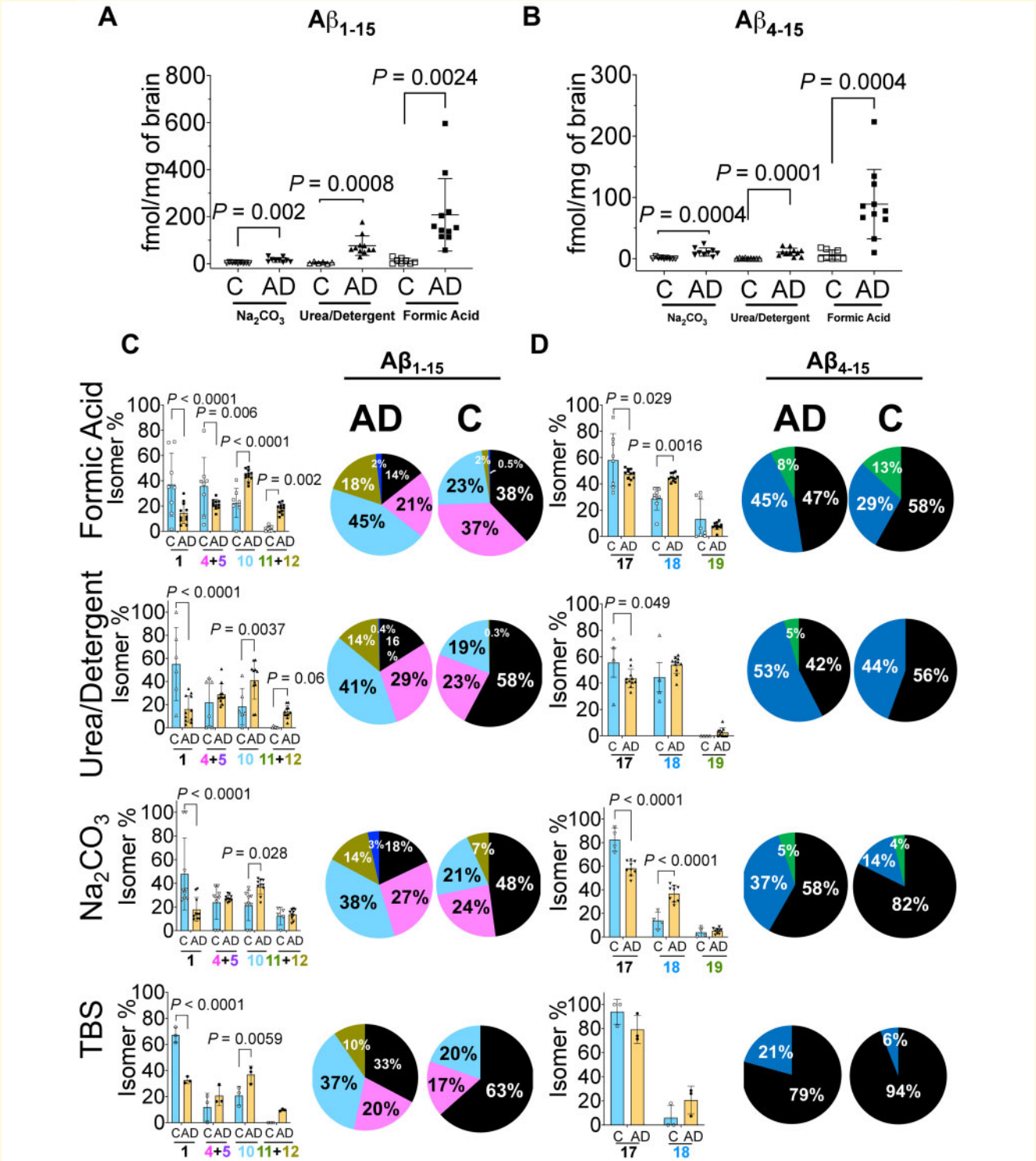

Figure 3 Quantitation of amyloid-β N-terminus isomers. Scatter plots for the absolute quantitation of the N-terminus of Aβ peptides (**A**) total $Aβ_{1–15}$ and (**B**) total $Aβ_{4–15}$ in the three amyloid rich biochemical fractions of Na_2CO_3, urea-detergent and formic acid. Aβ peptides were compared between Alzheimer's disease ($n = 11$) and control ($n = 9$) using mass spectrometry. The total levels of $Aβ_{1–15}$ and $Aβ_{4–15}$ are significantly elevated in Alzheimer's disease tissue in all biochemical fractions. (**C**) Percentage ratio of most abundant $Aβ_{1–15}$ isomers and (**D**) $Aβ_{4–15}$ isomers in Alzheimer's disease compared to control brains across different biochemical fractions. The unmodified $Aβ_{1–15}$ (native) is significantly decreased in all the biochemical fractions while doubly isomerized 1-*iso*, 7-*iso*-Asp $Aβ_{1–15}$ (10) diastereomer is significantly increased. The $Aβ_{4–15}$ isomer ratios demonstrated statistically significant changes in FA and Na_2CO_3 fractions. The pie charts summarize the pattern of distribution of isomerization of $Aβ_{1–15}$ and $Aβ_{4–15}$ in the different biochemical fractions. All the values are mean ± SD; significance in total $Aβ_{1–15}$ and $Aβ_{4–15}$ was determined by unpaired *t*-test with equal variance, while for the total amount of the $Aβ_{1–15}$ and $Aβ_{4–15}$ isomers and their normalized ratios, adjusted *p* values were calculated with ANOVA as described in the Materials and methods section. AD = Alzheimer's disease; C = control, individual isomers of $Aβ_{1–15}$ and $Aβ_{4–15}$ are numbered according to Fig. 2.

disease and control brain tissues was estimated using SIS peptides (Fig. 1C). As expected, total $A\beta_{1-15}$ was significantly increased in Alzheimer's disease brains (12-fold) compared to control brains, while 14-fold increase was documented for the total $A\beta_{4-15}$ (Table 1). Comparison of $A\beta_{1-15}$ and $A\beta_{4-15}$ revealed a significant elevation in these peptides in Alzheimer's disease across all four biochemical fractions (Table 1). Quantitative estimates of total $A\beta_{1-15}$ in the FA fraction revealed a significant elevation (20-fold increase, $P = 0.0024$), while 15-fold ($P = 0.0008$) and 4-fold ($P = 0.0021$) increase were observed in urea-detergent fraction and Na_2CO_3 fraction (Table 1, Fig. 3A), respectively. Due to low abundance of Aβ in the control group, we had to pool the TBS fractions for both the Alzheimer's disease as well as controls cases. Pooled soluble TBS fraction indicated a 4-fold ($P = 0.0365$) elevation of $A\beta_{1-15}$ in Alzheimer's disease brains (Table 1, Supplementary Fig. 8 A). Similarly, total $A\beta_{4-15}$ was significantly increased (~13-fold, $P = 0.0004$) in FA fraction, ~25-fold increase ($P = 0.0001$) in urea-detergent fraction and ~12-fold increase ($P = 0.0004$) in Na_2CO_3 fraction (Table 1, Fig. 3B). Interestingly, we observed ~29-fold increase ($P = 0.0263$) in $A\beta_{4-15}$ levels in the pooled Alzheimer's disease TBS fraction (Supplementary Fig. 8 A). The $A\beta_{4-15}/A\beta_{1-15}$ ratio in the FA and Na_2CO_3 fractions was at ~0.4 and 0.7, respectively, while this ratio in urea-detergent fraction was ~0.1 (Table 1, Fig. 2A and B). This indicates preferential accumulation of $A\beta_{4-15}$ in the insoluble/fibrillar and vesicular fractions in Alzheimer's disease brains consistent with its increased hydrophobicity.[53] The $A\beta_{4-15}/A\beta_{1-15}$ ratios in the insoluble pool indicated an increased accumulation of truncated Aβ with Phe-4 (phenylalanine residue) N-terminus in Alzheimer's disease, reaching almost equal concentration as the BACE1 cleaved Aβ N-terminus (Asp-1), making it the next most abundant N-termini present in Alzheimer's disease brains.

Next, we asked how much of total $A\beta_{1-15}$ and $A\beta_{4-15}$ was isomerized in each biochemical fraction in Alzheimer's disease in comparison to the control tissue. As expected, we observed significant elevation in the total amount of the isomers of $A\beta_{1-15}$ and isomers of $A\beta_{4-15}$ in each of the Aβ rich fractions from Alzheimer's disease tissue (Supplementary Fig. 9). Interestingly, even in the pooled Alzheimer's disease TBS fraction (soluble Aβ), we not only observed a significant decrease in the unmodified 1-L, 7-L-Asp $A\beta_{1-15}$ (1) peptide, but statistically significant elevation for the singly isomerized 1-*iso*-L, 7-L-Asp (4), 1-L, 7-*iso*-L-Asp (5) and doubly isomerized 1,7-*iso*-L-Asp $A\beta_{1-15}$ (10) peptides (Supplementary Fig. 8B).

In order to understand how the isomerization of Asp-1 and Asp-7 was associated with Alzheimer's disease, we investigated the changes in the total percentage of each isomer/epimer across the biochemical fractions (Fig. 3C and D). The percentage of isomerized to unmodified $A\beta_{1-15}$ indicated significant decrease of the native 1-L, 7-L-Asp (1) peptide with the concomitant statistically significant increase in 1-*iso*-L-Asp, 7-*iso*-L-Asp $A\beta_{1-15}$ (10) isomer in all the biochemical fractions in Alzheimer's disease (Fig. 3C). Overall, ~85% of $A\beta_{1-15}$ was detected in its isomerized form in the amyloid-rich fractions of Alzheimer's disease, while controls showed up to 50% isomerization depending on the pathology (Fig. 3C, Supplementary Fig. 10). Quantitatively, ~50% isomer 10 in the most amyloid-rich fractions of Alzheimer's disease brains compared to 20–27% in controls (Fig. 3C) was documented. Furthermore, we observed ~21–30% $A\beta_{1-15}$ with either Asp-1 or Asp-7 isomerized in Alzheimer's disease. In contrast, in controls singly isomerized Asp-1 or Asp-7 $A\beta_{1-15}$ are the predominant species in the FA fractions (~37%, $P = 0.006$) (Fig. 3C). These data indicated an increased isomerization event of $A\beta_{1-15}$ in Alzheimer's disease brain for an extended period of time. Strikingly, even the TBS soluble $A\beta_{1-15}$ present in the Alzheimer's disease brains demonstrated ~70% isomerization (~37% isomer 10, $P = 0.0059$) compared to only ~30% in controls (Fig. 3C).

Similarly, the proportion of isomerized $A\beta_{4-15}$ was elevated in Alzheimer's disease brain (Supplementary Fig. 8B). There was a significant increase of 7-*iso*-L-Asp $A\beta_{4-15}$ (18 in Fig. 3D) in FA (45%, $P = 0.0016$) and Na_2CO_3 (37%, $P < 0.0001$) fractions. Most importantly, there was an increase (~21%) in the amount of 7-*iso*-L-Asp $A\beta_{4-15}$ (18 in Fig. 3D) in the soluble TBS fractions of Alzheimer's disease brains compared to control brains (Fig. 3D). We also observed a distinct pattern of compartmentalization of highly isomerized Aβ in the insoluble fractions, while the soluble TBS pool had a higher percentage of unmodified peptide (Fig. 3C and D).

The potential influence of age at death on the accumulation of isomerized Aβ in the Alzheimer's disease brains was evaluated. As expected, the total levels of $A\beta_{1-15}$ and $A\beta_{4-15}$ were positively correlated with the age at death in the Alzheimer's disease brains (Supplementary Fig. 11) but not in control brains (Supplementary Fig. 12). However, no correlations with the isomer ratios of $A\beta_{1-15}$ or $A\beta_{4-15}$ were observed in Alzheimer's disease or controls (Supplementary Figs. 11 and 12). These results corroborate the spontaneous non-enzymatic reaction as the primary mechanism for the generation of these isomers on long-lived Aβ in the brains (not artefact of sample preparation).

Aβ mid-domain and C-terminus quantitation

We hypothesized the $A\beta_{28-42}$ and $A\beta_{28-40}$ quantitation would provide information about the distribution of the most common type of Aβ accumulating in the Alzheimer's disease brain tissue as it is generally assumed $A\beta_{42}$ is the predominate neuronal form of the peptide.[18,54] The absolute quantitation of $A\beta_{28-42}$ and $A\beta_{28-40}$ peptides was used to determine the ratio of

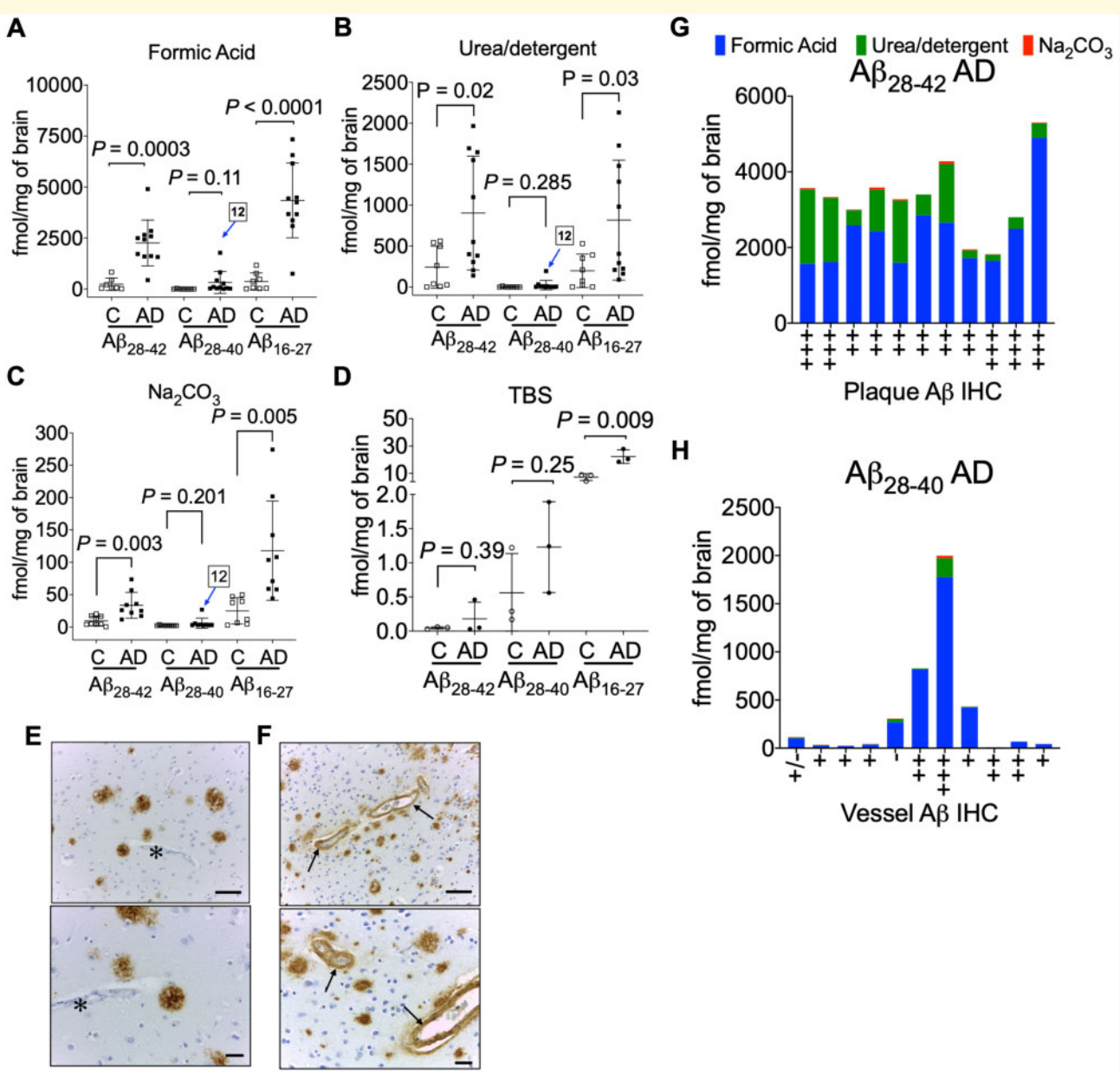

Figure 4 Quantitation of amyloid-β C-terminus. Scatter plots for the absolute quantitation of C-terminal $A\beta_{28–42}$, $A\beta_{28–40}$ and mid-domain $A\beta_{16–27}$ in the (**A**) FA, (**B**) urea-detergent, (**C**) Na_2CO_3 and (**D**) soluble TBS fractions from 9 controls and 11 Alzheimer's disease brains (temporal cortex). Pooled TBS homogenates (three replicates of pooled control and pooled Alzheimer's disease) were used to estimate the $A\beta_{28–42}$, $A\beta_{28–40}$ and mid-domain $A\beta_{16–27}$ levels. The levels of $A\beta_{16–27}$ were significantly elevated in Alzheimer's disease in all the biochemical fractions, while $A\beta_{28–42}$ was significantly elevated in FA, urea-detergent and Na_2CO_3 fractions. No statistical alteration was found in the levels of $A\beta_{28–40}$ in Alzheimer's disease compared to controls. AD12 indicates the patient with a high $A\beta_{28–40}$ level compared to others in all the amyloid-enriched biochemical fractions. Representative immunohistochemistry (IHC) images demonstrating Aβ amyloid staining in (**E**) typical Alzheimer's disease plaques without any vascular amyloid (asterisk) and (**F**) plaques and the intima of small blood vessels (arrows) from patient AD12 with the unusually high $A\beta_{28–40}$ level. Scale bar = 100 μm. (**G**) Total $A\beta_{28–42}$ levels compared to the amyloid plaque burden and (H) total $A\beta_{28–40}$ levels compared to vessel amyloid quantification from IHC. All the values are mean ± SD; significance in total $A\beta_{28–42}$, $A\beta_{28–40}$ and $A\beta_{16–27}$ was determined by unpaired *t*-test with equal variance. AD = Alzheimer's disease; C = control.

$A\beta_{40}/A\beta_{42}$ peptides across all the biochemical fractions (Supplementary Fig. 13). The quantitative estimates of $A\beta_{28–42}$ in the FA fraction was 2259 ± 1123 fmol/mg of brain in Alzheimer's disease tissue versus 233.7 ± 303 fmol/mg (Fig. 4A) in control brain (~10-fold increase $P = 0.0003$). In the urea-detergent fraction, we documented only a 3-fold increase ($P = 0.0207$) of $A\beta_{28–42}$ (Table 1, Fig. 4B) in Alzheimer's disease brain (903.9 ± 695.3 fmol/mg brain) compared to control brain (324.4 ± 255.8 fmol/mg brain). The $A\beta_{28–42}$ SISCAPA

quantitation in the Na_2CO_3 fraction indicated a ~3.5-fold increase ($P = 0.0001$) (Table 1, Fig. 4C) in Alzheimer's disease brain compared to control brain. Total $A\beta_{28–42}$ in the controls with pathology exhibited a range from 400 to 1400 fmol/mg brain (Supplementary Fig. 14) compared to 400 fmol/mg in non-pathological controls. Most interestingly, although there was more $A\beta_{28–40}$ in Alzheimer's disease compared to control tissue, it did not reach statistical significance in all of the biochemical fractions (Table 1). Strong correlation between $A\beta_{28–42}$ and $A\beta_{16–27}$ levels was found in the amyloid-rich biochemical fractions (Supplementary Fig. 15), while $A\beta_{28–40}$ did not correlate with $A\beta_{16–27}$ levels (Supplementary Fig. 16). This was driven by the high levels of $A\beta_{28–42}$, the predominant C-terminal peptide that accumulates in sporadic Alzheimer's disease brains.

As the decrease in the ratio of $A\beta_{42}/A\beta_{40}$ in the biological fluids (CSF/blood) has been shown to inversely correlate with brain amyloid PET imaging,[55,56] we next compared the ratio of $A\beta_{28–42}$ and $A\beta_{28–40}$ (Table 1, Supplementary Fig. 13). We did not find a corresponding increase in the $A\beta_{42}/A\beta_{40}$ ratio in FA or urea-detergent fractions but observed a statistically significant increase in $A\beta_{42}/A\beta_{40}$ ratio in the Na_2CO_3 fraction in Alzheimer's disease brains (Supplementary Fig. 13). This suggests the mechanisms that decrease $A\beta_{42}$ levels in CSF are disconnected with corresponding peptide levels in the brain. During our analysis, we observed an individual with highly elevated $A\beta_{28–40}$ in one Alzheimer's disease brain tissue (case 12, Fig. 4A–C). The high level of $A\beta_{28–40}$ correlated with the presence of prominent perivascular Aβ-amyloidosis for this case (Fig. 4F), as has been previously reported.[54,57] While the total $A\beta_{28–42}$ (3300 ± 974 fmol/mg brain) was consistent in Alzheimer's disease patients (Fig. 4G), significant increase in $A\beta_{28–40}$ was observed with prominent perivascular Aβ-amyloidosis (Fig. 4H).

Discussion

The slowly progressive nature of Alzheimer's disease with almost 20 years of Aβ accumulation from threshold to the onset of dementia predisposes the depositing Aβ peptide to undergo multiple biochemical changes at the molecular level. We used a quantitative proteomics approach coupled with ion mobility mass spectrometry to unravel the diversity of isomerized Aβ N-termini found in the Alzheimer's disease brain. Our major findings include (i) characterization of isomerization of the Asp residues (Asp-1 and Asp-7) in four common sequentially truncated N-termini of Aβ found in Alzheimer's disease brain tissues; (ii) quantitative estimation of the level of $A\beta_{1–15}$ and $A\beta_{4–15}$ in the biochemical pools with significant elevation in the Alzheimer's disease brain tissue; (iii) evaluation of the isomer ratios of $A\beta_{1–15}$ and $A\beta_{4–15}$, with significant elevation in doubly isomerized $A\beta_{1–15}$ and isomerized $A\beta_{4–15}$ levels in the insoluble/fibrillar and membrane pools, while the sparsely populated vesicular and soluble Aβ pools have lower proportion of these PTMs; (iv) brain-derived Aβ primarily has Ala-42 as the C-terminus which is significantly increased in Alzheimer's disease, while Aβ with Val-40 C-terminus is increased in Alzheimer's disease but does not reach statistical significance compared to control brains.

Iso-aspartate formation is one of the most common modifications associated with long-lived proteins/peptides.[22,58] The rate of *iso*-Asp formation in model peptides is considerably slower (half-life $t_{1/2}$, 53–266 days depending on the sequence) compared to asparagine deamidation/isomerization ($t_{1/2}$, 1.4 days). *In vitro*, the N-terminus of Aβ has been documented to undergo such spontaneous isomerization at Asp1 and Asp7 residues.[23] Slow reaction rates ($t_{1/2} \sim 231$ days, Asp-1; $t_{1/2} \sim 462$ days, Asp-7 for $A\beta_{1–40}$)[12] along with decreased fractional clearance rates in the CNS of Alzheimer's disease (28 ng/h $A\beta_{1–42}$ deposition)[5,59] can be used to estimate the age of the depositing isomerized peptides. Pathological controls with ~50% isomerized $A\beta_{1–15}$ (one $t_{1/2}$) indicate that the observed mild Aβ deposit (diffuse plaques) is nearly 8 months old. In contrast, data from the ~85% isomerized $A\beta_{1–15}$ (three $t_{1/2}$) in Alzheimer's disease (Fig. 3C), indicate that the age of this peptide is at least 4 years. Similarly, the age of $A\beta_{4–15}$ in Alzheimer's disease is nearly 1.2 years compared to 6 months in control brains. Interestingly, the rate of racemization of L-Asp to D-Asp was originally used to estimate 30 years for plaques formation.[60] Further investigation using better modelling of Aβ biogenesis and altered clearance rates observed in Alzheimer's disease patients would yield better estimates for these long-lived PTMs.

Along with N-terminal Asp isomerization, sequential truncated isoforms of Aβ such as $A\beta_{pGlu}$ have been well documented from different biochemical pools of Alzheimer's disease brain.[61] All of these PTMs have been linked to the hypothesis of how Aβ is toxic to neurons. However, they do not completely address the underlying feature of how or what causes the accumulation of Aβ to occur. Structural reorganization of the peptide chain due to Asp isomerization leads to alteration in the biochemical and physical properties of the peptide. Our data indicate that internal Asp residue isomerization reorients the peptide backbone, leading to changes in the shape and size of these Aβ peptides (Fig. 2) compared to unmodified ones in the gas phase. One of the possible links between the more stable long-lived isomerized/epimerized Aβ[62] and neurotoxicity could stem from their inherent resistance to enzymatic degradation by primary cathepsin found in the lysosomes.[12] Aβ residues 1–11 are predicted to play a critical role in the antigen recognition by antibodies targeting the N-terminus of Aβ peptide.[63–65] It has been suggested that N-terminus of Aβ is the dominant epitope, exposed on the surface of aggregated fibrillary deposits, while Aβ mid-domain drives oligomerization and toxicity.[66] Antibodies that target N-terminus are

considered competent in reducing Aβ deposits, while antibodies to mid-domain epitopes[67,68] should abrogate the toxic oligomers. Despite considerable reduction in Aβ (lowering of Aβ-PET signal) by monoclonal antibodies primarily to the Aβ N-terminus,[33,34,69] active and passive immunotherapy trials have largely failed to reach their primary end points.[70] Our data suggest, antibodies targeting the mid-domain Aβ might prove efficacious as it has very little PTM, while specifically targeting the older isomerized Aβ N-terminus for clearance will be better strategy for immunotherapy. Designing better therapeutic antibodies against modified Aβ would need further investigation into the structural properties of these PTMs and their influence on the antibody-mediated target engagement.

It has been postulated that the hydrophobic C-terminus of Aβ is responsible for inducing membrane permeability,[71] while the N-terminal domain induces innate immune responses from the microglia. Interestingly, it has been found that *iso*-Asp-7 $A\beta_{42}$ compared to wild-type $A\beta_{42}$ led to significantly increased phosphorylation of proteins, including tau (MAPT) from SH-SY5Y neuroblastoma cell-culture models.[72] Accumulation of iso-aspartate in proteins is known to be lethal in the PIMT (protein iso-aspartate methyltransferase) deficient mouse, suffering from progressive epileptic seizures.[73,74] Soluble Aβ oligomers isolated from Alzheimer's disease brains have been shown to induce hyperexcitability in individual neurons and neuronal circuits[75–77] Induction of hyperexcitability has been invoked to explain the clinical observation that there is a significantly higher incidence of epilepsy in Alzheimer's disease patients compared to age-matched controls.[78,79] Our results indicate that soluble $A\beta_{1–15}$ derived from Alzheimer's disease brain is significantly isomerized (~50% doubly isomerized, 20% singly isomerized) compared to soluble $A\beta_{1–15}$ (~20% doubly isomerized, 17% singly isomerized) in age-matched control brains (Fig. 3C). It would be interesting to quantitatively estimate how much of these Alzheimer's disease brain-derived soluble Aβ oligomers are isomerized at the N-terminus.

While we documented abundant N-terminal Asp-1 and Asp-7 isomerization/racemization in all the four different biochemical pools in both Alzheimer's disease and control brains (Fig. 3, Supplementary Fig. 10), surprisingly no modified $A\beta_{16–27}$ was observed (Supplementary Fig. 7). The presence of unique $A\beta_{16–27}$ species points to two major revelations: (i) N-terminus of Aβ is conformationally flexible allowing spontaneous reactions to occur and (ii) contrary to previous reports,[9,80] Asp-23 is unmodified in sporadic Alzheimer's disease. This indicates that this residue could either be solvent in-accessible or involved in H-bonding interactions precluding it from succinimide-mediated isomerization. With the current resolution of $R \sim 50$ for our DT-IMS-MS method, it is not possible to rule out any other amino acid (such as Ser) isomerization on this peptide. Future investigations with techniques like SLIM-IMS providing higher resolution ($R > 300$)[46,47] will lead to better understanding and characterization of other low abundant structural PTMs of Aβ in Alzheimer's disease brains.

The data presented here and by others[13,59,81–83] is consistent with $A\beta_{42}$ being the dominant neuronal peptide form accumulating in Alzheimer's disease brain with $A\beta_{40}$ levels increasing with perivascular amyloidosis.[54] Label-free intact MS has estimated that ~70% of Aβ depositing in the Alzheimer's disease brain has Ala-42 as the C-terminus compared to ~10% terminating at Val-40.[13] Historically, the majority of the peptide originally sequenced from the plaque-derived amyloid was $A\beta_{4–42}$.[7] Our results indicate that Aβ peptides depositing specifically in the insoluble pools of Alzheimer's disease brain have approximately equal amounts of BACE-1 cleaved Aβ (Asp-1 as the N-terminus) and ragged N-terminus peptide (Phe-4 residue) (Table 1, Fig. 3). Interestingly, recent MALDI-MS imaging of post-mortem Alzheimer's disease tissues with congophilic amyloid angiopathy (CAA) provided a distinct qualitative pattern of N- and C-terminal variations of deposited Aβ—extracellular plaques in the cerebral parenchyma were enriched with $A\beta_{42}$ while the vessels had less aggregation prone $A\beta_{40}$.[83–85] Quantitative estimation of $A\beta_{42}$ and $A\beta_{40}$ in biochemically defined pools from the temporal cortex of sporadic Alzheimer's disease revealed less than 0.01% of total $A\beta_{42}$ and 0.3% of total $A\beta_{40}$ are in the soluble cytosolic TBS fraction with the rest being distributed in either the vesicular (1.1% $A\beta_{42}$, 1.7% $A\beta_{40}$), membranous (28.3% $A\beta_{42}$, 6.8% $A\beta_{40}$) and/or insoluble fully polymerized fibrillar phase (70.7% $A\beta_{42}$, 91.2% $A\beta_{40}$). In contrast, total $A\beta_{42}$ in control brain tissue (0.5 ± 1.8 pmol/mg brain) is much lower concentrated compared to Alzheimer's disease brain (3.2 ± 1.8 pmol/mg brain). Again, most of the $A\beta_{42}$ is still partitioned in the membranous (57.2%) and insoluble/fibrillar fraction (41.2%). Drugs that can target the C-terminus,[86] specifically $A\beta_{42}$ for clearance have much better chance to exploit the equilibrium of amyloid deposition in Alzheimer's disease brain.

Development of therapeutic drugs and interventions for ameliorating or decreasing the progress of Alzheimer's disease requires techniques that can accurately and quantitatively monitor the changes in the amyloid biomarkers in the CSF and/or the blood along with PET imaging. Our results show that isomerized Aβ is intricately associated with the accumulation of $A\beta_{42}$ in the brain—a key distinguishing signature from freshly generated Aβ. Future studies will be required to understand the role of these isomers in the disease, but this is clearly an important question to answer due to the >80% abundance of isomerized Aβ in Alzheimer's disease brain.

Conclusion

In summary, in this study we have shown that different biochemical pools of Aβ has different amounts of N-

terminus isomerization. Insoluble plaques and membrane fractions in Alzheimer's disease brains have ~85% isomerized $A\beta_{1-15}$, while vesicular and soluble fractions have lower percentage of isomerization. The extent of isomerization on Aβ extracted from Alzheimer's disease brains is 3 years older than the Aβ found in age-matched control brains. Quantitatively, BACE-1-cleaved Asp-1 N-terminus is present in almost equimolar amounts with Phe-4 truncated N-terminus, an interesting Aβ metabolic by-product of unclear origin. Our data provide the link between older isomerized Aβ and the consequences it might have in the disease aetiology, such as oligomers that diffuse out of these plaques into soluble pool will be neurotoxic due to their inherent resistance to lysosomal degradation. Strategies in designing better immunotherapeutic must take into consideration of the extensive PTMs of the N-terminus of Aβ and specifically target older isomerized Aβ species for better target engagement and clearance.

Supplementary material

Supplementary material is available at *Brain Communications* online.

Acknowledgements

We thank the Agilent Technologies for the 6560 IM-MS qToF instrument, Melbourne Mass Spectrometry and Proteomics Facility of The Bio21 Molecular Science and Biotechnology Institute at The University of Melbourne for the support of qualitative bottom-up and ETD-PRM mass spectrometry analysis. We thank Fairlie Hinton and Geoff Pavey with human brain tissues from the Brain Bank.

Funding

Funding was from National Health and Medical Research Council (NHMRC) Dementia Leadership Fellowship (B.R.R., APP1138673), NHMRC project (B.R.R., APP1164692), and Alzheimer's Drug Discovery Foundation (ADDF).

Competing interests

B.R.R. receives research support from Agilent Technologies. All other authors declare no competing interests.

References

1. Braak H, Braak E. Neuropathological stageing of Alzheimer-related changes. Acta Neuropathol. 1991;82(4):239–259.
2. Villemagne VL, Burnham S, Bourgeat P, et al. Amyloid beta deposition, neurodegeneration, and cognitive decline in sporadic Alzheimer's disease: a prospective cohort study. Lancet Neurol. 2013;12(4):357–367.
3. Bateman RJ, Munsell LY, Morris JC, Swarm R, Yarasheski KE, Holtzman DM. Human amyloid-beta synthesis and clearance rates as measured in cerebrospinal fluid in vivo. Nat Med. 2006;12(7):856–861.
4. Mawuenyega KG, Sigurdson W, Ovod V, et al. Decreased clearance of CNS beta-amyloid in Alzheimer's disease. Science. 2010;330(6012):1774.
5. Roberts BR, Lind M, Wagen AZ, et al. Biochemically-defined pools of amyloid-beta in sporadic Alzheimer's disease: correlation with amyloid PET. Brain. 2017;140(5):1486–1498.
6. Hardy J, Selkoe DJ. The amyloid hypothesis of Alzheimer's disease: progress and problems on the road to therapeutics. Science. 2002;297(5580):353–356.
7. Masters CL, Simms G, Weinman NA, Multhaup G, McDonald BL, Beyreuther K. Amyloid plaque core protein in Alzheimer disease and Down syndrome. Proc Natl Acad Sci USA. 1985;82:4245–4249.
8. Goedert M, Spillantini MG, Cairns NJ, Crowther RA. Tau proteins of Alzheimer paired helical filaments: abnormal phosphorylation of all six brain isoforms. Neuron. 1992;8(1):159–168.
9. Shimizu T, Watanabe A, Ogawara M, Mori H, Shirasawa T. Isoaspartate formation and neurodegeneration in Alzheimer's disease. Arch Biochem Biophys. 2000;381(2):225–234.
10. Truscott RJW, Schey KL, Friedrich MG. Old proteins in man: a field in its infancy. Trends Biochem Sci. 2016;41(8):654–664.
11. Kozin SA, Cheglakov IB, Ovsepyan AA, et al. Peripherally applied synthetic peptide isoAsp7-Abeta(1–42) triggers cerebral beta-amyloidosis. Neurotox Res. 2013;24(3):370–376.
12. Lambeth TR, Riggs DL, Talbert LE, et al. Spontaneous isomerization of long-lived proteins provides a molecular mechanism for the lysosomal failure observed in Alzheimer's disease. ACS Cent Sci. 2019;5(8):1387–1395.
13. Wildburger NC, Esparza TJ, LeDuc RD, et al. Diversity of amyloid-beta proteoforms in the Alzheimer's disease brain. Sci Rep. 2017;7(1):9520.
14. Kummer MP, Hermes M, Delekarte A, et al. Nitration of tyrosine 10 critically enhances amyloid beta aggregation and plaque formation. Neuron. 2011;71(5):833–844.
15. Kuo YM, Emmerling MR, Woods AS, Cotter RJ, Roher AE. Isolation, chemical characterization, and quantitation of A beta 3-pyroglutamyl peptide from neuritic plaques and vascular amyloid deposits. Biochem Biophys Res Commun. 1997;237(1):188–191.
16. Mandler M, Walker L, Santic R, et al. Pyroglutamylated amyloid-beta is associated with hyperphosphorylated tau and severity of Alzheimer's disease. Acta Neuropathol. 2014;128(1):67–79.
17. Rijal Upadhaya A, Kosterin I, Kumar S, et al. Biochemical stages of amyloid-beta peptide aggregation and accumulation in the human brain and their association with symptomatic and pathologically preclinical Alzheimer' disease. Brain. 2014;137(Pt 3):887–903.
18. Naslund J, Schierhorn A, Hellman U, et al. Relative abundance of Alzheimer A beta amyloid peptide variants in Alzheimer disease and normal aging. Proc Natl Acad Sci USA. 1994;91(18):8378–8382.
19. Vazquez de la Torre A, Gay M, Vilaprinyo-Pascual S, et al. Direct evidence of the presence of cross-linked Abeta dimers in the brains of Alzheimer's disease patients. Anal Chem. 2018;90(7):4552–4560.
20. Bada JL, Helfman PM. Amino acid racemization dating of fossil bones. World Archaeol. 1975;7(2):160–173.
21. McCudden CR, Kraus VB. Biochemistry of amino acid racemization and clinical application to musculoskeletal disease. Clin Biochem. 2006;39(12):1112–1130.
22. Geiger T, Clarke S. Deamidation, isomerization, and racemization at asparaginyl and aspartyl residues in peptides. Succinimide-

linked reactions that contribute to protein degradation. J Biol Chem. 1987;262(2):785–794.
23. Lyons B, Friedrich M, Raftery M, Truscott R. Amyloid plaque in the human brain can decompose from Abeta(1–40/1–42) by spontaneous nonenzymatic processes. Anal Chem. 2016;88(5): 2675–2684.
24. Shapira R, Austin GE, Mirra SS. Neuritic plaque amyloid in Alzheimer's disease is highly racemized. J Neurochem. 1988;50(1): 69–74.
25. Kummer MP, Heneka MT. Truncated and modified amyloid-beta species. Alzheimers Res Ther. 2014;628-(3).
26. Azizeh BY, Head E, Ibrahim MA, et al. Molecular dating of senile plaques in the brains of individuals with Down syndrome and in aged dogs. Exp Neurol. 2000;163(1):111–122.
27. Inoue K, Hosaka D, Mochizuki N, et al. Simultaneous determination of post-translational racemization and isomerization of N-terminal amyloid-beta in Alzheimer's brain tissues by covalent chiral derivatized ultraperformance liquid chromatography tandem mass spectrometry. Anal Chem. 2014;86(1):797–804.
28. Roher AE, Lowenson JD, Clarke S, et al. beta-Amyloid-(1–42) is a major component of cerebrovascular amyloid deposits: implications for the pathology of Alzheimer disease. Proc Natl Acad Sci USA. 1993;90(22):10836–10840.
29. Roher AE, Kokjohn TA, Clarke SG, et al. APP/Abeta structural diversity and Alzheimer's disease pathogenesis. Neurochem Int. 2017;110:1–13.
30. Polanco JC, Li C, Bodea L-G, Martinez-Marmol R, Meunier FA, Götz J. Amyloid-beta and tau complexity - towards improved biomarkers and targeted therapies. Nat Rev Neurol. 2018;14(1): 22–39.
31. van Dyck CH. Anti-amyloid-beta monoclonal antibodies for Alzheimer's disease: pitfalls and promise. Biol Psychiatry. 2018; 83(4):311–319.
32. Zhang Y, Zou J, Yang J, Yao Z. 4Abeta1-15-derived monoclonal antibody reduces more Abeta burdens and neuroinflammation than homologous vaccine in APP/PS1 mice. Curr Alzheimer Res. 2015;12(4):384–397.
33. Sevigny J, Chiao P, Bussiere T, et al. The antibody aducanumab reduces Abeta plaques in Alzheimer's disease. Nature. 2016; 537(7618):50–56.
34. Vandenberghe R, Rinne JO, Boada M, et al. Bapineuzumab for mild to moderate Alzheimer's disease in two global, randomized, phase 3 trials. Alzheimers Res Ther. 2016;8(1):18.
35. González LJ, Shimizu T, Satomi Y, et al. Differentiating alpha- and beta-aspartic acids by electrospray ionization and low-energy tandem mass spectrometry. Rapid Commun Mass Spectrom. 2000;14(22):2092–2102.
36. Lehmann WD, Schlosser A, Erben G, Pipkorn R, Bossemeyer D, Kinzel V. Analysis of isoaspartate in peptides by electrospray tandem mass spectrometry. Protein Sci. 2000;9(11):2260–2268.
37. Cournoyer JJ, Pittman JL, Ivleva VB, et al. Deamidation: differentiation of aspartyl from isoaspartyl products in peptides by electron capture dissociation. Protein Sci. 2005;14(2):452–463.
38. Sargaeva NP, Lin C, O'Connor PB. Identification of aspartic and isoaspartic acid residues in amyloid beta peptides, including Abeta1–42, using electron-ion reactions. Anal Chem. 2009;81(23): 9778–9786.
39. Tao Y, Quebbemann NR, Julian RR. Discriminating D-amino acid-containing peptide epimers by radical-directed dissociation mass spectrometry. Anal Chem. 2012;84(15):6814–6820.
40. Du S, Readel ER, Wey M, Armstrong DW. Complete identification of all 20 relevant epimeric peptides in beta-amyloid: a new HPLC-MS based analytical strategy for Alzheimer's research. Chem Commun. 2020;56(10):1537–1540.
41. Wu C, Siems WF, Klasmeier J, Hill HH. Jr., Separation of isomeric peptides using electrospray ionization/high-resolution ion mobility spectrometry. Anal Chem. 2000;72(2):391–395.
42. de Magalhaes MT, Barbosa EA, Prates MV, et al. Conformational and functional effects induced by D- and L-amino acid epimerization on a single gene encoded peptide from the skin secretion of *Hypsiboas punctatus*. PLoS One. 2013;8(4):e59255.
43. Jia C, Lietz CB, Yu Q, Li L. Site-specific characterization of (D)-amino acid containing peptide epimers by ion mobility spectrometry. Anal Chem. 2014;86(6):2972–2981.
44. Jeanne Dit Fouque K, Garabedian A, Porter J, et al. Fast and effective ion mobility–mass spectrometry separation of d-amino-acid-containing peptides. Anal Chem. 2017;89(21):11787–11794.
45. Li G, DeLaney K, Li L. Molecular basis for chirality-regulated Abeta self-assembly and receptor recognition revealed by ion mobility-mass spectrometry. Nat Commun. 2019;10(1):5038.
46. Zheng X, Deng L, Baker ES, Ibrahim YM, Petyuk VA, Smith RD. Distinguishing d- and l-aspartic and isoaspartic acids in amyloid beta peptides with ultrahigh resolution ion mobility spectrometry. Chem Commun. 2017;53(56):7913–7916.
47. Nagy G, Kedia K, Attah IK, et al. Separation of beta-amyloid tryptic peptide species with isomerized and racemized l-aspartic residues with ion mobility in structures for lossless ion manipulations. Anal Chem. 2019;91(7):4374–4380.
48. Anderson NL, Anderson NG, Haines LR, Hardie DB, Olafson RW, Pearson TW. Mass spectrometric quantitation of peptides and proteins using stable isotope standards and capture by anti-peptide antibodies (SISCAPA). J Proteome Res. 2004;3(2): 235–244.
49. Ippoliti PJ, Kuhn E, Mani DR, et al. Automated microchromatography enables multiplexing of immunoaffinity enrichment of peptides to greater than 150 for targeted MS-based assays. Anal Chem. 2016;88(15):7548–7555.
50. May JC, Knochenmuss R, Fjeldsted JC, McLean JA. Resolution of isomeric mixtures in ion mobility using a combined demultiplexing and peak deconvolution technique. Anal Chem. 2020; 92(14): 9482–9492.
51. Schilling B, Rardin MJ, MacLean BX, et al. Platform-independent and label-free quantitation of proteomic data using MS1 extracted ion chromatograms in skyline: application to protein acetylation and phosphorylation. Mol Cell Proteomics. 2012;11(5):202–214.
52. Sargaeva NP, Lin C, O'Connor PB. Differentiating N-terminal aspartic and isoaspartic acid residues in peptides. Anal Chem. 2011;83(17):6675–6682.
53. Cabrera E, Mathews P, Mezhericher E, et al. Abeta truncated species: implications for brain clearance mechanisms and amyloid plaque deposition. Biochim Biophys Acta Mol Basis Dis. 2018; 1864(1):208–225.
54. Gkanatsiou E, Portelius E, Toomey CE, et al. A distinct brain beta amyloid signature in cerebral amyloid angiopathy compared to Alzheimer's disease. Neurosci Lett. 2019;701:125–131.
55. Nakamura A, Kaneko N, Villemagne VL, et al. High performance plasma amyloid-beta biomarkers for Alzheimer's disease. Nature. 2018;554(7691):249–254.
56. Schindler SE, Bollinger JG, Ovod V, et al. High-precision plasma beta-amyloid 42/40 predicts current and future brain amyloidosis. Neurology. 2019;93e1647–e59. (17):
57. Charidimou A, Boulouis G, Gurol ME, et al. Emerging concepts in sporadic cerebral amyloid angiopathy. Brain. 2017;140(7): 1829–1850.
58. Stephenson RC, Clarke S. Succinimide formation from aspartyl and asparaginyl peptides as a model for the spontaneous degradation of proteins. J Biol Chem. 1989;264(11):6164–6170.
59. Patterson BW, Elbert DL, Mawuenyega KG, et al. Age and amyloid effects on human central nervous system amyloid-beta kinetics. Ann Neurol. 2015;78(3):439–453.
60. Muller-Hill B, Beyreuther K. Molecular biology of Alzheimer's disease. Annu Rev Biochem. 1989;58:287–307.
61. Perez-Garmendia R, Gevorkian G. Pyroglutamate-modified amyloid beta peptides: emerging targets for Alzheimer's disease immunotherapy. Curr Neuropharmacol. 2013;11(5):491–498.

62. Bohme L, Hoffmann T, Manhart S, Wolf R, Demuth HU. Isoaspartate-containing amyloid precursor protein-derived peptides alter efficacy and specificity of potential beta-secretases. Biol Chem. 2008;389(8):1055–1066.
63. Gardberg AS, Dice LT, Ou S, et al. Molecular basis for passive immunotherapy of Alzheimer's disease. Proc Natl Acad Sci U.S.A. 2007;104(40):15659–15664.
64. Bohrmann B, Baumann K, Benz J, et al. Gantenerumab: a novel human anti-Abeta antibody demonstrates sustained cerebral amyloid-beta binding and elicits cell-mediated removal of human amyloid-beta. J Alzheimers Dis. 2012;28(1):49–69.
65. Arndt JW, Qian F, Smith BA, et al. Structural and kinetic basis for the selectivity of aducanumab for aggregated forms of amyloid-beta. Sci Rep. 2018;8(1):6412.
66. Petkova AT, Ishii Y, Balbach JJ, et al. A structural model for Alzheimer's beta -amyloid fibrils based on experimental constraints from solid state NMR. Proc Natl Acad Sci USA. 2002;99(26):16742–16747.
67. Doody RS, Thomas RG, Farlow M, et al. Phase 3 trials of solanezumab for mild-to-moderate Alzheimer's disease. N Engl J Med. 2014;370(4):311–321.
68. Yang T, Dang Y, Ostaszewski B, et al. Target engagement in an Alzheimer trial: crenezumab lowers amyloid beta oligomers in cerebrospinal fluid. Ann Neurol. 2019;86(2):215–224.
69. Ostrowitzki S, Lasser RA, Dorflinger E, et al. A phase III randomized trial of gantenerumab in prodromal Alzheimer's disease. Alzheimers Res Ther. 2017;9(1):95.
70. Panza F, Lozupone M, Logroscino G, Imbimbo BP. A critical appraisal of amyloid-beta-targeting therapies for Alzheimer disease. Nat Rev Neurol. 2019;15(2):73–88.
71. Ciudad S, Puig E, Botzanowski T, et al. Abeta(1–42) tetramer and octamer structures reveal edge conductivity pores as a mechanism for membrane damage. Nat Commun. 2020;11(1):3014.
72. Zatsepina OG, Kechko OI, Mitkevich VA, et al. Amyloid-beta with isomerized Asp7 cytotoxicity is coupled to protein phosphorylation. Sci Rep. 2018;8(1):3518.
73. Yamamoto A, Takagi H, Kitamura D, et al. Deficiency in protein L-isoaspartyl methyltransferase results in a fatal progressive epilepsy. J Neurosci. 1998;18(6):2063–2074.
74. Qin Z, Dimitrijevic A, Aswad DW. Accelerated protein damage in brains of PIMT+/- mice; a possible model for the variability of cognitive decline in human aging. Neurobiol Aging. 2015;36(2):1029–1036.
75. Lei M, Xu H, Li Z, et al. Soluble Abeta oligomers impair hippocampal LTP by disrupting glutamatergic/GABAergic balance. Neurobiol Dis. 2016;85:111–121.
76. Brinkmalm G, Hong W, Wang Z, et al. Identification of neurotoxic cross-linked amyloid-beta dimers in the Alzheimer's brain. Brain. 2019;142(5):1441–1457.
77. Zott B, Simon MM, Hong W, et al. A vicious cycle of beta amyloid-dependent neuronal hyperactivation. Science. 2019;365(6453):559–565.
78. Amatniek JC, Hauser WA, DelCastillo-Castaneda C, et al. Incidence and predictors of seizures in patients with Alzheimer's disease. Epilepsia. 2006;47(5):867–872.
79. Vossel KA, Ranasinghe KG, Beagle AJ, et al. Incidence and impact of subclinical epileptiform activity in Alzheimer's disease. Ann Neurol. 2016;80(6):858–870.
80. Shimizu T, Fukuda H, Murayama S, Izumiyama N, Shirasawa T. Isoaspartate formation at position 23 of amyloid beta peptide enhanced fibril formation and deposited onto senile plaques and vascular amyloids in Alzheimer's disease. J Neurosci Res. 2002;70(3):451–461.
81. Kang J, Lemaire HG, Unterbeck A, et al. The precursor of Alzheimer's disease amyloid A4 protein resembles a cell-surface receptor. Nature. 1987;325(6106):733–736.
82. Iwatsubo T, Odaka A, Suzuki N, Mizusawa H, Nukina N, Ihara Y. Visualization of A beta 42(43) and A beta 40 in senile plaques with end-specific A beta monoclonals: evidence that an initially deposited species is A beta 42(43). Neuron. 1994;13(1):45–53.
83. Di Fede G, Catania M, Maderna E, et al. Molecular subtypes of Alzheimer's disease. Sci Rep. 2018;8(1):3269.
84. Kakuda N, Miyasaka T, Iwasaki N, et al. Distinct deposition of amyloid-beta species in brains with Alzheimer's disease pathology visualized with MALDI imaging mass spectrometry. Acta Neuropathol Commun. 2017;5(1):73.
85. Michno W, Nystrom S, Wehrli P, et al. Pyroglutamation of amyloid-betax-42 (Abetax-42) followed by Abeta1–40 deposition underlies plaque polymorphism in progressing Alzheimer's disease pathology. J Biol Chem. 2019;294(17):6719–6732.
86. Landen JW, Cohen S, Billing CB, Jr, et al. Multiple-dose ponezumab for mild-to-moderate Alzheimer's disease: safety and efficacy. Alzheimers Dement. 2017;3(3):339–347.